Biophysical Journal Volume 92 February 2007 977–988

Structure and Molecular Mechanism of *Bacillus anthracis* Cofactor-Independent Phosphoglycerate Mutase: A Crucial Enzyme for Spores and Growing Cells of *Bacillus* Species

Masatoshi Nukui,* Luciane V. Mello,[†‡] James E. Littlejohn,* Barbara Setlow,[§] Peter Setlow,[§] Kijeong Kim,* Terrance Leighton,* and Mark J. Jedrzejas*

*Children's Hospital Oakland Research Institute, Oakland, California 94609; [†]Northwest Institute for Bio-Health Informatics/University of Liverpool, Liverpool L69 7ZB, United Kingdom; [‡]Embrapa Recursos Genéticos e Biotecnologia, Brasília, DF, Brazil; and [§]Department of Molecular, Microbial and Structural Biology, University of Connecticut Health Center, Farmington, Connecticut 06030

ABSTRACT Phosphoglycerate mutases (PGMs) catalyze the isomerization of 2- and 3-phosphoglycerates and are essential for glucose metabolism in most organisms. This study reports the production, structure, and molecular dynamics analysis of *Bacillus anthracis* cofactor-independent PGM (iPGM). The three-dimensional structure of *B. anthracis* PGM is composed of two structural and functional domains, the phosphatase and transferase. The structural relationship between these two domains is different than in the *B. stearothermophilus* iPGM structure determined previously. However, the structures of the two domains of *B. anthracis* iPGM show a high degree of similarity to those in *B. stearothermophilus* iPGM. The novel domain arrangement in *B. anthracis* iPGM and the dynamic property of these domains is directly linked to the mechanism of enzyme catalysis, in which substrate binding is proposed to result in close association of the two domains. The structure of *B. anthracis* iPGM and the molecular dynamics of this structure provide unique insight into the mechanism of iPGM catalysis, in particular the roles of changes in coordination geometry of the enzyme's two bivalent metal ions and the regulation of this enzyme's activity by changes in intracellular pH during spore formation and germination in *Bacillus* species.

INTRODUCTION

Phosphoglycerate mutases (PGMs) catalyze the isomerization of 2- and 3-phosphoglycerates (2PGA and 3PGA) and are essential for glucose metabolism in most organisms (1,2). There are two evolutionarily distinct classes of PGMs (1)—those dependent on the cofactor 2,3-bisphosphoglycerate (dPGMs) and those whose activity is independent of this cofactor but dependent on divalent metal cations, most often Mn^{2+} cofactor-independent phosphoglycerate mutase (iPGMs). Regulation of the activity of iPGM during sporulation and spore germination in *Bacillus* species, and probably *Clostridium* species as well, is very important as the developing spore accumulates a large depot of 3PGA whose catabolism provides a significant amount of the ATP needed in the first 10 min of spore outgrowth (3,4). The activity of the 57-kDa monomeric iPGM from *Bacillus* species absolutely and specifically requires Mn^{2+} and is exquisitely pH sensitive. At a Mn^{2+} concentration of 20 μM the activity of this enzyme decreases more than 100-fold, going from pH 7.7 to pH 6.5 (5). The exquisite pH sensitivity of this enzyme's activity seems almost certain to be due to the pH sensitivity of the binding of the enzyme's essential Mn^{2+} ions and also has physiological relevance (1,4,6,7). iPGM becomes inactive in the developing forespore of *Bacillus* species as the pH in this cellular compartment decreases to ~6.5, and this allows the developing spore to accumulate a large depot of 3PGA. This 3PGA is then utilized to generate ATP in the first 10–20 min of spore germination and outgrowth when the pH of the germinated spore rises to ~7.7, thus allowing rapid iPGM activity (1,3,7). The gene for iPGM from *B. stearothermophilus* has been cloned and the enzyme overexpressed and purified to homogeneity (8). The purification of this enzyme led to its crystallization and x-ray crystallographic structure determination of its complexes with 3PGA (6) and 2PGA (7). Two Mn^{2+} ions were present in each structure.

The structure of *B. stearothermophilus* iPGM has an $\tilde{\alpha}\beta$-type topology and is composed of two domains, termed the transferase and phosphatase, reflecting their roles in catalysis (6,7). Both domains have similar folds consisting of a central β-sheet structure flanked on both sides by α-helices, and the two domains interact through complementary surfaces that form a network of hydrogen-bond interactions. The residues binding both substrate and Mn^{2+} as well as the catalytic residues are located in the interdomain cleft (Fig. 1). The phosphate group of the substrate and the two Mn^{2+} ions interact primarily with the phosphatase domain, which also contains the catalytic Ser-62, whereas the glycerate part of PGA interacts only with the transferase domain (Fig. 2).

Comparison of the structure of the iPGM's phosphatase domain with structures of alkaline phosphatase (AlkP) (9) and sulfatase (10,11) showed that these enzymes have a common core structure and revealed similarly located conserved Ser (in iPGM and AlkP) or Cys (in sulfatases) residues and two divalent metal ions in the active sites (12).

Submitted July 24, 2006, and accepted for publication October 13, 2006.

Address reprint requests to Mark J. Jedrzejas, Children's Hospital Oakland Research Institute, 5700 Martin Luther King Jr. Way, Oakland, CA 94609. Tel.: 510-450-7932; Fax: 510-450-7914; E-mail: mjedrzejas@chori.org.

0006-3495/07/02/977/12 $2.00

doi: 10.1529/biophysj.106.093872

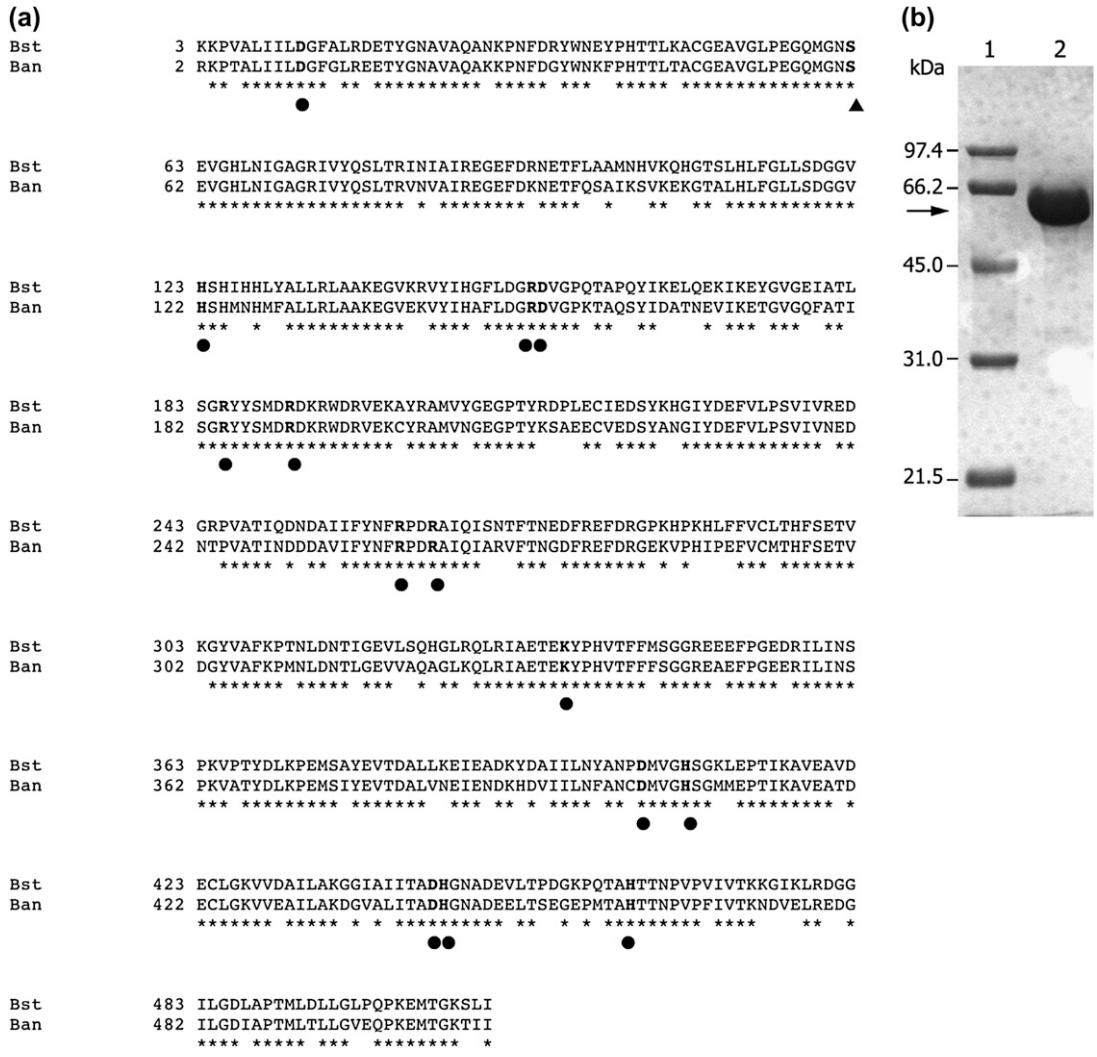

FIGURE 1 Sequence analysis and production of *B. anthracis* iPGM. (*a*) Alignment of sequences of *B. anthracis* and *B. stearothermophilus* iPGMs. The overall sequence identity is 78%; however, in the phosphatase domain the identity increased to 79%, and for the transferase domain decreased to 74%. Conserved residues are marked by an asterisk, the residues of the catalytic site are marked by solid circles with the exception of catalytic Ser-61, which is marked by a solid triangle. (*b*) Electrophoretic analysis. Coomassie brilliant blue stained 10% SDS-PAGE gel: lane 1, protein molecular mass standards; lane 2, 3s mg of purified *B. anthracis* iPGM.

Sequence comparisons identified other enzymes in the AlkP superfamily—autotaxin (containing a catalytic, Thr residue which is phosphorylated), phosphopentomutase, phosphoglycerol transferase, phosphonoacetate hydrolase, and the GPI-anchoring enzymes (glycosylphosphatidylinositol phosphoethanolamine transferases) MCD4, GPI7, and GPI13 (12). Therefore, structural and mechanistic investigation of iPGM will likely be relevant to a large group of enzymes belonging to the same superfamily.

Early biochemical studies of wheat germ iPGM provided strong support for an intramolecular mutase reaction in which intermediates remain bound to the enzyme (13–15). These results and stereochemical data related to active site Mn^{2+} (16) have been interpreted in terms of a mechanism involving the formation of a phosphoenzyme intermediate. Structural and site-directed mutagenesis studies were in full accord with this notion (1,17), suggesting the formation of a phosphoenzyme intermediate at the active site residue Ser-62. Mn^{2+} ions play an essential role in this reaction through coordination of the substrate, product, and phosphoserine intermediate (6,7). The crucial role for the two Mn^{2+} ions in iPGM catalysis also leads to the extreme pH sensitivity of this reaction, which is crucial for both accumulation of 3PGA in sporulation and 3PGA catabolism during spore germination (1,18,19).

Previous work with *Bacillus* species has shown that i), these bacteria do not contain a dPGM, ii), their iPGM is essential for rapid growth and for sporulation, and iii), lack of an iPGM sensitizes cells to glucose (20–22). The metabolic importance of iPGMs for these bacteria and the apparent absence of iPGMs in vertebrates including humans make this class of enzyme an attractive therapeutic target

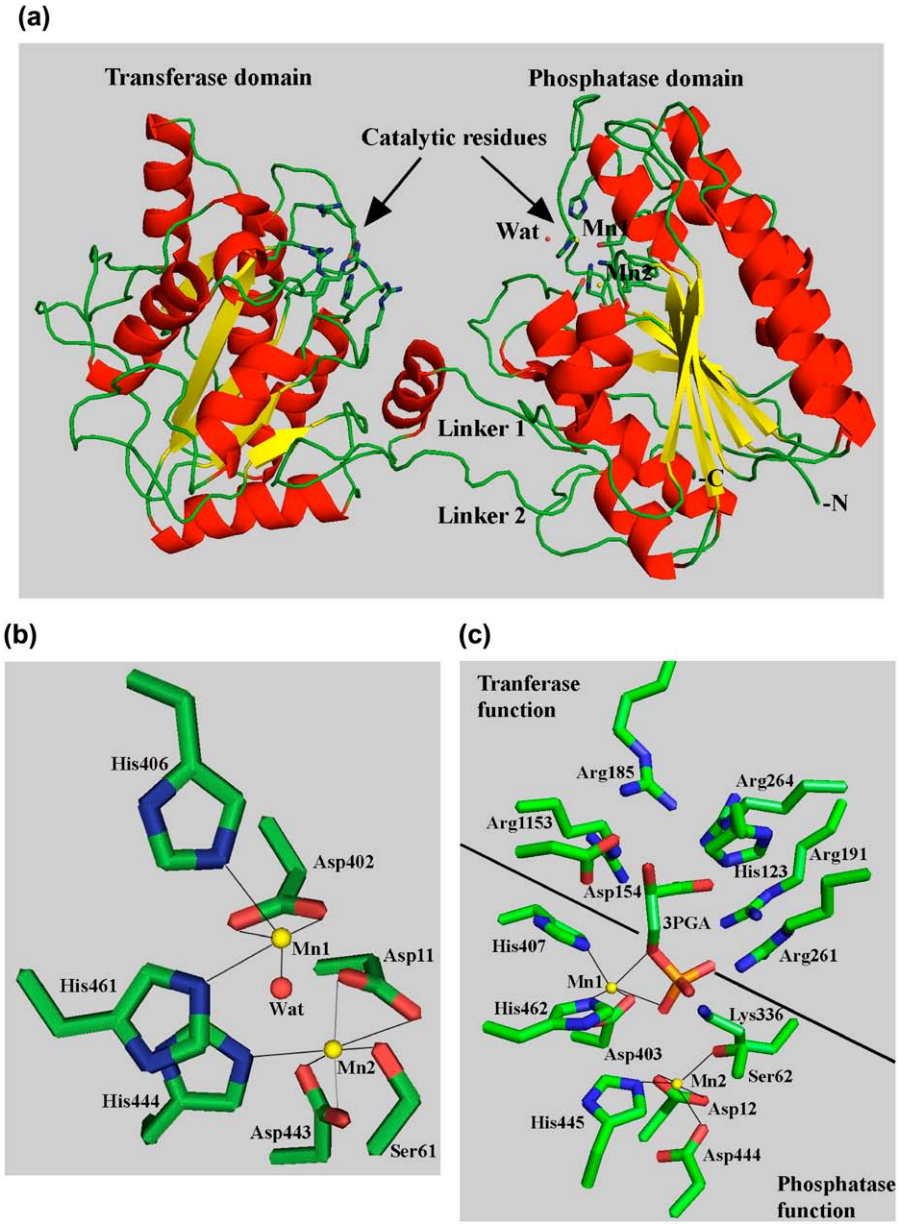

FIGURE 2 Three-dimensional structure of *B. anthracis* iPGM. (*a*) Overall ribbon representation of the molecule. This single peptide chain molecule assumes a two-domain structure with phosphatase and transferase domains. These domains are connected by two short peptide linkers, linker1 and 2. The structure is color coded by secondary structure elements: helices, red; β-sheets, yellow; and loops, green. Both N- and C-termini are labeled. The active site residues are shown in a ball and stick fashion (color-coded by element: carbon, *green*; oxygen, *red*; and nitrogen, *blue*). These residues belong to the two separate domains, phosphatase and transferase. For catalysis, these domains must move within reach of one another. The total of 13 amino acid residues take part in catalysis together with two essential Mn^{2+} ions, Mn^1 and Mn^2, and one water molecule, Wat. (*b*) Coordination spheres of catalytic Mn^{2+} ions. The coordination sphere of both the Mn^{2+} ions differs from that of distorted square pyramidal observed for *B. stearothermophilus* iPGM bound to PGA. For the *B. anthracis* iPGM without PGA, Mn^1 assumes a distorted square pyramidal coordination but the apex has moved from NE2 of His-461 to a different ligand. Mn^2 is in distorted octahedral coordination, altered from a distorted square pyramidal coordination, with the apex at OG of Ser-61. The atoms occupying the apex positions are NE2 of His-406 for Mn^1 (distorted square pyramidal coordination), and OD1 of Asp-11 and OD2 of Asp-443 for Mn^2 (distorted octahedral coordination). (*c*) Structure of catalytic site of *B. stearothermophilus* iPGM. This iPGM was crystallized with both domains close together with its catalytic residues in functional positions as during enzyme catalysis. A 3PGA substrate/product molecule is also shown. The residue numbering scheme follows that of *B. anthracis* iPGM enzyme plus one (i.e., *B. anthracis* Ser-61 is equivalent to *B. stearothermophilus* Ser-62). The coordination spheres of both Mn^{2+} ions were also depicted utilizing thin lines. The coordination geometry for both ions is distorted square pyramidal with NE2 of His-462 and OG of Ser-62 occupying the apex positions for Mn^1 and Mn^2, respectively (6).

(22–26). Design of drugs targeting iPGM of *Bacillus* species is particularly attractive given the concerns over the use of spores of *B. anthracis* as an aerosolized bioweapon. A necessary first step in the structure-based design of drugs is the determination of a three-dimensional structure of *B. anthracis* iPGM, the subject of this article.

MATERIAL AND METHODS

Cloning and overexpression

The iPGM coding sequences of *B. anthracis* strain Ames (27) (GenBank Accession No. NC_003997 region: complement (4859710..4861239)) and *B. anthracis* strain Sterne (GenBank Accession No. NC_005945, region: complement (4861047..4862576)) were identified with Blast protein queries using the *B. stearothermophilus* (28) iPGM amino acid sequence as reported (8) (GenBank Accession No. AF120091). The sequences of the proteins from both *B. anthracis* strains were identical. For expression of a native form of *B. anthracis* iPGM, an N-terminal fusion vector, pTYB11 (New England Biolabs, Beverly, MA) was used. This vector contains a T7/*lac* promoter and an intein tag, which is self-cleavable when exposed to thiols such as 1,4-dithiothreitol (DTT), β-mercaptoethanol, or cysteine, and carries a chitin-binding domain for purification of the fusion precursor by affinity chromatography (29). The intein tag encodes the chitin-binding domain, and after on-column cleavage of the tag, the protein dissociates from the column. PCR primers for iPGM were designed using Oligo V6.5 primer design software, (MBI, Cascade, CO), employing coding and flanking sequences. The primer sequences were forward primer, 5′-ATGAGAAAGCCAACAGC-3′; reverse primer, 5′-GCGAGCATAAACATCAAT-3′. Pwo DNA polymerase (Roche Molecular Systems, Indianapolis, IN), a proofreading

polymerase was employed for PCR amplification, using purified *B. anthracis* strain Sterne 34-F2genomic DNA. PCR and cloning procedures were similar to those used for *B. stearothermophilus* iPGM (8). The cloned iPGM coding sequence had identical DNA sequence to those of the two *B. anthracis* GenBank accessions.

Overexpression and purification of native *B. anthracis* iPGM

The sequence-verified plasmid was transformed into *Escherichia coli* BL21(DE3) (Invitrogen, Carlsbad, CA) and BL21-CodonPlus (DE3)-RP (Stratagene, La Jolla, CA) competent cells according to the manufacturers' protocols. Optimal conditions for high-level expression of the intein-iPGM fusion protein were determined by preliminary small-scale expression studies under various conditions. The cells were grown in RM medium (1× M9 salts, 2% casamino acids, 1% glycerol, 1 mM $MgCl_2$, pH 7.0) (29) containing 100 μg/mL ampicillin and 50 μg/mL chloramphenicol at 37°C with shaking at 250 rpm (30). After the culture reached an OD_{600} of 0.8–1, protein expression was induced by adding isopropyl-β-D-thiogalactopyranoside (IPTG) to a final concentration of 1 mM with further incubation at 15°C for 36 h. The induced cells were harvested by centrifugation at 5000 × *g* for 10 min at 4°C, and the cell pellet was resuspended in 300 mL ice-cold cell lysis buffer (20 mM Tris-HCl (pH 8.5), 500 mM NaCl, 1 mM Tris-(2-carboxyethly) phosphine (TCEP), 1 mM EDTA, 20 μM phenylmethanesulfonyl fluoride). The resuspended cells were disrupted by sonication at 4°C, and the suspension centrifuged at 20,000 × *g* for 30 min at 4°C. The fusion protein (intein-iPGM) in the supernatant fluid was isolated by chitin affinity purification at 4°C, and iPGM was recovered by on-column cleavage (31) at 23°C and eluted with binding buffer at 4°C. The eluted iPGM fractions were analyzed by 10% sodium dodecylsulfate-polyacrylamide gel electrophoresis (SDS-PAGE) as described (32). The recovered iPGM was dialyzed at 4°C against 10 mM Tris-HCl (pH 7.4), 100 mM KCl, 5 mM $MnCl_2$, 1 mM DTT, 50 μM EDTA. Protein was concentrated at 4°C using an Ultrafree-15 centrifugal filter device (Millipore, Bedford, MA).

Crystallization and diffraction data collection

B. anthracis iPGM produced as described above had a specific activity similar to that of *B. stearothermophilus* iPGM (see Results) (4,8). The protein was concentrated to 25 mg/mL in 10 mM Tris-HCl (pH 7.4), 100 mM KCl, 5 mM $MnCl_2$, 1 mM DTT, and 50 μM EDTA. For crystallization the hanging drop vapor diffusion method was employed (33); equal volumes (1 μL each) of the enzyme and reservoir solution were utilized, plus 1 μL of additive solution. The reservoir solution contained 24% (w/v) polyethylene glycol 8000 (PEG8000), 100 mM Tris-HCl (pH 7.2), and 200 mM calcium acetate, and the additive solution contained 3% (w/v) 1,5-diaminopentane di-HCl in water. Crystals grew within several weeks and were of irregular elongated rectangular plate morphology. The crystals were cryoprotected utilizing PEG8000 and glycerol (28% (w/v) and 25% (v/v), respectively) and frozen using standard methodology. The diffraction data were collected using a synchrotron source, the x-ray beam wavelength of 1.1 Å at beamline 5.0.1 of the Berkeley Center for Structural Biology, Advanced Light Source, Lawrence Berkeley National Laboratory. An ADSC (Area Detector Systems Corp., Poway, CA) Quantum 4u charge-coupled device detector was used and the data were collected in oscillation mode (34). The crystals yielded an x-ray diffraction data set extending to 2.42-Å resolution and indexed to an orthorhombic $P2_12_12_1$ space group with unit cell dimensions $a = 43.62$, $b = 72.82$, and $c = 184.92$ Å (Table 1).

Structure solution and refinement

The structure of *B. anthracis* iPGM was solved by molecular replacement methods employing the Phaser program (35,36) and utilizing the 1.70-Å crystal structure of *B. stearothermophilus* iPGM (Protein Data Bank (PDB) code 2eqj; (6,7)) as a search model. It was necessary for this search model structure to be divided into two smaller parts, based on structural domains identified in our earlier studies (6,7), to obtain a satisfactory solution. Once obtained the solution was further refined exploiting rigid body refinement in refmac5 (37) and manual mutation and/or rebuilding with O (38). Refinement proceeded by alternating rounds of maximum likelihood computational refinement implemented in refmac5 (37) and manual rebuilding with O (38). All data were used with no intensity or σ-based cutoffs applied. σA-weighted map coefficients (39) were used throughout. An R_{free} value (40), calculated from 5% of reflections set aside at the outset, was used to monitor the progress of refinement. Water molecules were placed into 3σ positive peaks in $|F_o - F_c|$ maps when density was also evident in $|2F_o - F_c|$ maps and suitable hydrogen-bonding partners were available. Molecules derived from the crystallization and cryoprotecting solutions, primarily glycerol, were modeled into suitably shaped regions of electron density. Final statistics for the two structures are given in Table 1. Programs of the CCP4 package (37) were used for all x-ray diffraction data and three-dimensional structure manipulations. The final structure was analyzed utilizing Procheck (41) and Sfcheck (42). All structure figures were made with PYMOL (43), Grasp (44), or O software (38).

TABLE 1 X-ray diffraction data parameters and final structure refinement statistics

Space group	$P2_12_12_1$
Unit cell	
a (Å)	43.62
b (Å)	72.82
c (Å)	184.92
Low resolution diffraction limit (Å)	50.00
High resolution diffraction limit (Å)	2.40
Completeness*	91.8 (84.2)
I/σ(I)*	9.9 (2.1)
Multiplicity (%)	3.2 (2.9)
R_{merge}* (%)	10.8 (44.3)
Number of nonhydrogen protein atoms	3907
Number of nonhydrogen solvent atoms	184
Number of Mn^{2+} ions	2
Number of reflections	22,459
Number of reflections above 3σ(I)	14,828
R (%)*	24.5 (29.8)
R_{free} (%)*	29.8 (43.3)
Mean temperature factor *B* All atoms (Å^2)	53.3
Protein	53.4
Protein main chain	52.9
Protein side chain	56.7
Mn^{2+} ions	44.8
Solvent	51.1
RMSD from ideal values	
Bond lengths (Å)	0.007
Bond angles (°)	1.5

*Values in brackets are for the highest resolution shell 2.49–2.40 Å.

Flexibility analysis

Molecular dynamics (MD) simulations of 10 ns each were performed on three different systems. The crystal structure of iPGM from *Bacillus stearothermophilus* complexed with Mn^{2+} and 2PGA (PDB code 1o98) (24) was used in the first simulation. The second MD run used the same system, but 2PGA was manually removed. The third MD simulation was performed with the crystal structure herein described, the open structure of *B. anthracis* iPGM bound to Mn^{2+} alone. The MD calculations employed the GROMACS simulation suite (45) using the force field appropriate for proteins in water. Sodium ions were added to the simulation system to compensate for the net negative charge of the protein and, where present, ligand. The simulation was carried out in a cubic box with a minimal distance between solute and box edge of 0.7 nm.

Periodic boundary conditions were used. The topology file for 2PGA was built using the small-molecule topology generator PRODRG (46), followed by manual examination. 2PGA was modeled in its trianionic form since it is in close proximity to metal ions in the *B. stearothermophilus* iPGM crystal structure. The essential dynamics (ED) method (47) is a powerful tool for filtering large-scale concerted fluctuations from an ensemble of conformations, e.g., an MD trajectory or a set of experimental structures. The method is equivalent to a principal component analysis and is based on the diagonalization of the covariance matrix of atomic fluctuations, which yields a set of eigenvalues and eigenvectors. The eigenvectors indicate directions in a 3 n-dimensional space (with n = the number of atoms of the protein) and describe concerted fluctuations of the atoms. The eigenvalues reflect the magnitude of the fluctuation along the respective eigenvectors. The DynDom program (47,48) was used to compare domain structural differences between the two systems. DynDom defines dynamic domains by comparison of two sets of protein coordinates. DynDom assigns rotation vectors for each domain, which together describe the transition from one conformation to the other. The minimum domain size assigned was 20 residues, minimum ratio 1.0, and the sliding window length used was 5 residues.

Other methods

The iPGM was assayed at 23°C using a one-step assay with 3PGA as the substrate, and coupling 2PGA formation to NADH oxidation with the enzymes enolase, pyruvate kinase, and lactate dehydrogenase plus ADP (4,49). $MnCl_2$ was present in the assays at 0.5 mM. The concentration of *B. anthracis* iPGM was determined from its ultraviolet absorption at 280 nm using the molar extinction coefficient calculated from the protein's amino acid sequence (8,50).

RESULTS AND DISCUSSION

Cloning and expression of *B. anthracis* iPGM

The amino acid sequence of *B. anthracis* strain Ames iPGM was quite similar to the iPGM of *B. stearothermophilus* (GenBank Accession No. AF120090), with 78% sequence identity (Fig. 1 *a*). The *B. anthracis* iPGM has 509 amino acids, two fewer than the *B. stearothermophilus* enzyme. The N-terminal Met residue was likely removed posttranslationally from the *B. anthracis* iPGM, as it is from *B. stearothermophilus* iPGM (3).

In initial attempts to overexpress iPGM, the level of the fusion protein (intein-iPGM) in BL21(DE3) cells was very low. We explored a variety of expression conditions to improve protein yields. It was possible that the high frequency of rare codons in the *B. anthracis* iPGM gene reduced expression in the host *E. coli* cells. Therefore specially engineered *E. coli* BL21-CodonPlus (DE3)-RP cells (Stratagene) containing tRNAs supporting rare codon expression (51) were used subsequently and allowed the successful overexpression of iPGM. Other modifications that facilitated high levels of iPGM expression were the utilization of RM medium, IPTG induction at 15°C, as well as a 36-h period for overexpression. Induction of expression at low temperature was crucial to prevent generation of insoluble iPGM. The expressed fusion protein was isolated using a chitin-affinity column and after on-column cleavage of the intein yielded a highly purified iPGM (Fig. 1 *b*). A total of ~12 mg of pure iPGM was obtained from 1 L of culture and was concentrated to 25 mg/mL for crystallization trials.

The purified *B. anthracis* iPGM converted 37 μmol 3PGA to 2PGA per mg protein in 1 min at 23°C, a temperature that was ~10°C below the optimum growth temperature for *B. anthracis*. This specific activity is higher than that determined for purified *B. stearothermophilus* iPGM at 65°C (15 mmol 3PGA converted to 2PGA/min·mg (6,8)), the optimum growth temperature of this thermophilic species.

Structure and its description

The crystal structure of *B. anthracis* iPGM at 2.40-Å resolution was solved using the structure of the *B. stearothermophilus* iPGM-2PGA complex (7) as the model for molecular replacement solution as described in Materials and Methods. This structure accounts for all residues of the produced protein except Met-1, which was presumably removed post-translationally. The structure also includes two catalytically important Mn^{2+} ions and 184 water molecules (Table 1). The side chains of several residues were not accounted for in the electron density and, therefore, they were truncated to Ala (Lys-284, Leu-312, Asp-313, Lys-500, Glu-501, and Lys-509) or Gly (Asn-311, Glu-283, Asp-280, and Lys-213) residues for final refinement of the model. The majority of these truncated residues are located at the surface-exposed regions, and none is within the enzyme's catalytic site (6). The final refinement statistics are summarized in Table 1. All residues of the final model are within energetically allowed regions, with 85.8% (374 residues) in the most favored region and 2.1% (9 residues) in a generously allowed one (41). Remaining residues were in additional allowed regions (53 residues, 12.1%). These latter nine residues are located in the loop areas on the protein surface and appear to take part in interactions primarily with other molecules in the crystal.

As in the *B. stearothermophilus* iPGM (6,7) the *B. anthracis* enzyme assumed a globular structure with two domains connected by two short linker peptides (Fig. 2 *a*). Each domain has a specialized function in the mutase reaction, with one domain responsible for a phosphatase reaction (phosphatase domain: Met-1–Ala-70 and Thr-315–Lys-509) and the other for phosphate transfer (transferase domain: Leu-78–Tyr-304). The linker peptides were composed of Gly-71–Ser-77 (linker 1) and Val-305–Asn-314 (linker2). The overall root mean-square (RMS) deviation between the iPGMs from the two *Bacillus* species is 7.1 Å. However, the structures of individual domains were much more similar between these two enzymes that were reflected in RMS deviation (RMSD) of 0.5 and 0.7 Å for the phosphatase and transferase domains, respectively. The folds of these domains were similar to each another and consisted of a central β-sheet surrounded by helices on both sides. This fold is also similar to that in *B. stearothermophilus* iPGM and was defined as α/β type (6,7,52). The vast majority of the residues that were truncated in the final structure due to the lack of corresponding electron density (see above) were those of the transferase domain or linker2. In the phosphatase domain only three residues' side

chains were truncated and they were located only at the C-terminus of this domain (and the entire protein) (Fig. 2 *a*).

A deep and wide cleft separates the two domains of the enzyme and makes them appear independent (Fig. 2). The surface of the sides of the cleft is built from loops extending between helical structures as well as central β-sheets of individual domains. The phosphatase domain contains two bound Mn^{2+} ions that were shown to be essential for the mutase reaction (6,7). The mutase reaction can be divided into the phosphatase reaction generating the short-lived phospho-Ser enzyme intermediate (phosphate group originating from the substrate) with the essential Mn^{2+} ions and the transferase part responsible for creation of a reoriented glycerate-phosphate product (1,6,7,17). The residues of the active site belong to both domains and are far apart in space due to the large separation of the two domains in the crystal structure of the enzyme. The residues responsible for the phosphatase or transferase functions are entirely located within the two respective domains (Fig. 2).

The active site

The active site comprises 15 amino acids: 8 from the phosphatase domain and participating in the phosphatase reaction, and the remaining 7 from the transferase domain and participating in reorientation of the glycerate part of the substrate and its rephosphorylation, two Mn^{2+} ions, and a water molecule. The iPGMs from *Bacillus* species as well as other spore-forming low G:C Gram-positive eubacteria have an essential and specific requirement for this divalent cation (4,8). In the *B. stearothermophilus* iPGM structures these two Mn^{2+} ions have distorted square pyramidal ligand coordination geometry (6,7,19). The apex coordination of Mn^1 was occupied by His-462 (His-461 for *B. anthracis* iPGM), and for Mn^2 the apex coordination was occupied by Ser-62 (Ser-61 for *B. anthracis* iPGM). In *B. anthracis* iPGM the geometry of the coordination spheres of these ions was different (Fig. 2 *b*). Mn^1 still assumed a distorted square pyramidal coordination, but the apex has moved to the NE2 atom of His-406. Mn^2, on the other hand, had a new coordination geometry which was distorted octahedral with two apexes present, one being the OD1 atom of Asp-11 (apex 1) and the other the OD2 oxygen of Asp-443 (apex 2). This Mn^2 coordination clearly exhibits the presence of the Jan-Teller effect in its bond length and angles (53) (Fig. 2 *b*, Table 2). In particular, shortened distances and distorted angles involving the two apexes are manifestations of this theorem at work. Briefly, the Jahn-Teller effect states that any nonlinear molecular system in a degenerate electronic state will be unstable and will undergo distortion lowering its symmetry and split the degenerate state. The major interactions evident

TABLE 2 Nonbonded interactions in the active site of *B. anthracis* iPGM

Metal	Ligand (residue)	Distance (Å)	Ligand-metal-ligand angle (°)				
			OD1 D-402	OD2 H-406	NE2 H-461	Wat-15	
Mn^1	NE2 (H-406)	2.41—apex	81.7	98.9	84.0	95.7	
Square	OD1 (D-402)	2.98		47.3	76.1	157.7	
Pyramidal	OD2 (D-402)	2.34			121.5	153.7	
	NE2 (H-461)	2.19				81.7	
	OH (Wat-15)	2.82					
			OD2 D-443	OD2 D-11	SG S-61	OD1 D-443	NE2 H-444
Mn^2	OD1 (D-11)	2.30—apex 1	115.4	47.1	101.8	75.7	107.8
Octahedral	OD2 (D-443)	2.23—apex 2		117.1	107.1	40.1	101.2
	OD2 (D-11)	2.93			101.7	71.3	150.7
	OG (S-61)	2.46				102.4	102.4
	OD1 (D-443)	2.94					89.3
	NE2 (H-444)	2.32					
Mn^1	Mn^2	4.99					

Atom (residue)	Atom (residue)	Distance (Å)
Phosphatase domain		
OD2 (D-11)	ND2 (N-393)	2.55
OG (S-61)	NZ (K-335)	2.75
NZ (K-335)	OD2 (D-402)	2.72
OD1 (D-402)	CE1 (H-444)	2.85
OH (Wat-15)	OH (Wat-118)	3.15
Transferase domain		
NE2 (H-122)	OH (Wat-57)	2.59
OD1 (D-153)	NH2 (R-184)	2.70
	OH (Wat-28)	2.52
OD2 (D-153)	OH (Wat-57)	2.56
NH1 (R-184)	ND1 (D-150)	2.88
	OD1 (D-153)	2.70
NH1 (R-260)	OH (Wat-34)	2.85
NH2 (R-260)	OH (Wat-140)	2.66

within the active site of *B. anthracis* iPGM are reported in Table 2. The active site also contains a water molecule that is structured and fills in the coordination sphere of Mn^1 during the catalytic cycle when substrate is not bound (6,7). In the earlier proposed mechanism for iPGM catalysis (6,7,52) substrate binding displaces this water molecule and this Mn^1 ligand is replaced by the oxygen atom of the substrate (ether oxygen bridging glycerate with phosphate's phosphorus). The substrate molecule fills this void as a Mn^1 ligand until the product leaves the active site and the water molecule moves back in. The details of the proposed mechanism for bacterial iPGM have been described earlier (6,7).

The significance of the altered coordination geometry of the binuclear metal center in *B. anthracis* iPGM is not clear but suggests that the enzyme may have the ability to alter this coordination during the various stages of catalysis. In addition, the utilization of Mn^{2+} ions by spore-forming bacterial iPGMs results in an exquisite pH sensitivity of iPGM catalysis, as noted in the introduction. This is important in sporulation, as the pH drops from a value of ~7.7 in vegetative cells and the mother cell compartment of the sporulating cell to ~6.5 in the developing forespore and dormant spore (3,54–56). This results in the inactivation of iPGM in the forespore and the accumulation of a large depot of 3PGA that is stored in the dormant spore (4). When spores return to life in the process of germination, the pH of the spore cytoplasm returns to ~7.7, thus reactivating iPGM and allowing the utilization of the stored 3PGA for production of ATP (4). The pH sensitivity of the iPGMs of *Bacillus* species has been attributed to the enzyme's use of Mn^{2+} ions and the enzyme's ability to modify the coordination geometry of the metal ions in a pH-sensitive manner to prevent or facilitate catalysis (1,6,7,17). Here, we have observed such a modification of the Mn^{2+} ion's environment, thus supporting our earlier suggestions.

Comparison with the structure of *B. stearothermophilus* iPGM: domain motion

All residues of the active site of *B. anthracis* iPGM, including those interacting with the binuclear Mn^{2+} ion center, were conserved when compared to *B. stearothermophilus* iPGM. Structural comparisons yield similar results, i.e., essentially identical placement of amino acid residues and Mn^{2+} ions, but only when comparing the catalytic residues of the phosphatase and transferase domains individually (data not shown) (Fig. 2, *a* and *c*). This is due to the large opening of the cleft located between the two domains in *B. anthracis* iPGM, as this opening is significantly larger than in the *B. stearothermophilus* iPGM structure and provides additional support for the independent functionality of the two domains.

The major novelty of the current structure is the evidence for the significant flexibility of iPGM leading to a large separation between the two domains of the structure. Our earlier flexibility analyses of the *B. stearothermophilus* enzyme revealed relatively small enzyme flexing leading to opening and closing of the aperture/gate, allowing for substrate/product entry into or leaving of the catalytic site located deep within the interdomain crevice (24). This study indicates that iPGM has the ability for greater flexibility than was suspected previously. The reasons for this behavior are not clear, but such dynamic behavior could facilitate enzymatic catalysis.

Both earlier structures of iPGM (from *B. stearothermophilus*) were obtained using complexes of iPGM with its substrate or product. A decrease in the concentration of PGA in the crystallization mixture below 150 mM resulted in the lack of crystal formation. In addition, these crystals could only be grown at temperatures of ~22°C, which is ~43°C below the optimum growth temperature of this thermophilic bacterium (8). The crystals of *B. anthracis* iPGM, however, were obtained only without the substrate/product and at ~22°C, which is only ~13°C below the optimum growth temperature for this bacterium.

Molecular dynamics analysis and flexibility of iPGM enzymes

To investigate the dynamic motion of iPGM, full-scale MD studies were performed. We produced three trajectories, two starting from the closed structure of *B. stearothermophilus* iPGM, one of the protein and divalent metals, the other also containing substrate 2PGA (6,7), modeled in a form bearing three negative charges. The third trajectory used the open structure of metal-bound *B. anthracis* iPGM as the starting model. The resultant stable components of each enzyme's MD trajectory were used for DynDom analysis and for the comparison of the structures of the closed and the opened forms of the enzyme. The superposition between these two crystal structures is depicted in Fig. 3 *a*, which illustrates in diagrammatic form the motion components/domain leading to the difference between the two structures. The motion of this enzyme's domain is essentially a rotation of the two domains (Fig. 3 *a*), where one moves with respect to the other around an axis defined by the vector perpendicular to the line between the centers of the two domains. Hinge residues are colored in green, and they largely correspond to linkers 1 and 2 described earlier. The first hinge region consists of residues Ile-73 to Arg-80, and the second residues Phe-307 to Leu-316 (*B. anthracis* iPGM numbering scheme). The rotation angle between the two domains is very large, 63.7°, and the translation reported by DynDom for the transition, 0.9 Å, is negligible. The transition between the two forms of iPGM, which in general can be a mixture of translation and/or rotation of one domain with respect to the other, is, in this case, an essentially pure rotation about a set of hinge residues, i.e., linker1 and 2. Significant flexibility of enzymes belonging to AlkP superfamily has been observed before, including flexibility of their subunits/domains. For *E. coli* AlkP, for example, such flexibility has been attributed to phosphate binding (57) or

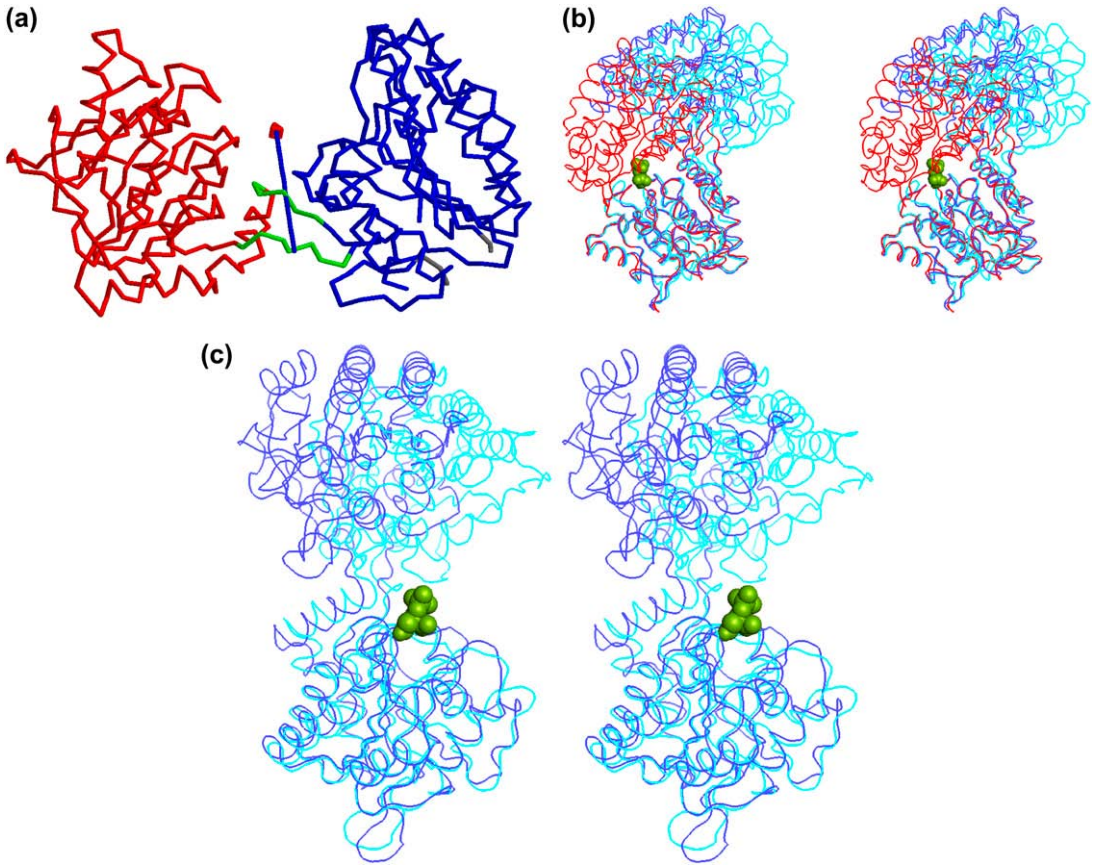

FIGURE 3 Comparison of iPGM structures and their dynamic properties. (*a*) Structural differences between structures of iPGMs of *Bacillus* species illustrated by DynDom analysis. Two domains (*red* and *blue*) are connected by hinge regions colored green. The arrow represents the axis of rotation of the two domains relative to each other. The structural difference between the two structures may be represented as a near pure rotation about the green hinge residues with negligible independent translation. (*b*) Stereo view of a superposition between the open (*dark blue*; based on the *B. anthracis* iPGM structure) and closed (*red*; based on the *B. stearothermophilus* iPGM structure) crystal structures and the average structure obtained from the stable portion of the open trajectory (*cyan*). The structures were superimposed using Cα atoms of the phosphatase domain alone. It is clear that the significant divergence of the average trajectory structure (*cyan*) from the initial open structure (*dark blue*) was not in the direction of the closed structure (*red*). (*c*) Superposition between the open structure and its average trajectory structure rotated 90° with respect to the orientation in *a*. 2PGA is presented in green. The difference between the average open structure during MD and the starting open crystal structure corresponds to a twisting of the phosphatase and mutase domains.

was metal induced (58). It, therefore, appears that large protein flexibility/movement is relevant to other enzyme of this superfamily than just iPGM.

During the MD simulation of the closed, PGA-bound *B. stearothermophilus* iPGM the structure remains within an RMSD of ~1.5 Å compared to the starting crystal structure, as illustrated in Fig. 4 *a*. The RMSD throughout the simulation of the closed structure, iPGM without PGA, remained lower to the closed *B. stearothermophilus* crystal form than to the open *B. anthracis* crystal structure, and deviated only slightly more from the starting structure than when ligand is present. Thus, it appears that there are barriers to the opening of the catalytic site that are independent of the presence of ligand. In contrast, Fig. 4 *a* also depicts that the MD simulation of the *B. anthracis* open iPGM conformation stabilizes after ~3 ns at an RMSD of ~5 Å compared to the starting structure. This difference was much greater than the deviation from crystal structure typically observed during MD. The shift was not toward the closed conformation—the RMSD compared to the closed *B. stearothermophilus* crystal structure fluctuates around 8–9 Å. Fig. 4, *b* and *c*, demonstrates the distances between key residues of the cleft, where the ligand binds, during the trajectory. There was little tendency for the substrate-binding cleft to close during the simulation of the open form of the *B. anthracis* enzyme, whereas the cleft remains closed in the closed *B. stearothermophilus* simulations.

An average structure derived from the 3–10-ns portion of the *B. anthracis* trajectory was compared to both crystal structures. Fig. 3, *b* and *c*, shows stereo views of the superposition between the open (*B. anthracis*) and closed (*B. stearothermophilus*) crystal structures and the average open *B. anthracis* structure along the simulation. The structures were superimposed using the phosphatase domain alone. As can be seen the difference between the average open structure during MD and the starting open crystal

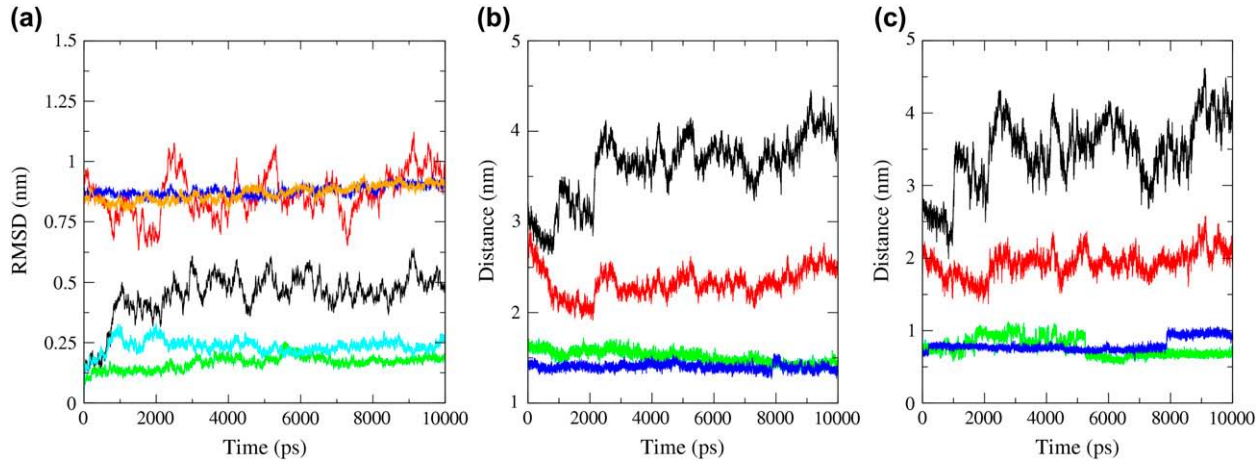

FIGURE 4 Geometric analyses of the simulations of open *B. anthracis* and closed *B. stearothermophilus* iPGM structures. (*a*) Cα RMS differences to open and closed structures. RMS values calculated using all Cα atoms. The open, closed, and closed (ligand artificially removed) simulations are compared to their respective starting structures in the black, green, and cyan traces, respectively. These traces show that the closed structure is stable during the simulation and only marginally less so when its ligand has been removed. In contrast, the open simulation stabilizes at a conformation significantly different (RMSD of ~0.5 nm) from the crystal structure. The upper traces, colored red, blue, and orange for the open, closed, and closed (ligand removed) (model structures) simulations show the cross comparisons of open simulations with closed structures and vice versa. They show that the fluctuations during the MD simulations do not cause the open simulations to more closely approximate the closed structures and vice versa. (*b*) Cα-Cα distances (nm) indicating the degree of closure of the catalytic site. For the simulation of closed *B. stearothermophilus* enzyme they are Lys-364 to Arg-153 (*blue*) or Lys-364 to Arg-264 (*green*). In the open *B. anthracis* simulation, the corresponding distances are Lys-363 to Arg-152 (*black*) and Lys-363 to Arg-263 (*red*). These distances measure the degree of closure of the catalytic site at the local level. They show that the catalytic site of the closed simulation remains closed throughout (*green* and *blue traces*), whereas the catalytic site of the open simulation is more conformationally variable but shows no tendency to close. (*c*) Additional Cα-Cα distances (nm) indicating the degree of closure of the catalytic site. The distances shown correspond to those depicted in panel *b* but measure the separation of the side-chain atoms Lys NZ and Arg CZ (nm) rather than the separation of their Cα atoms.

structure corresponded to a twisting of the phosphatase and mutase domains, rather than a closure to better approximate the closed crystal structure. This result is in agreement with the RMS analysis depicted by Fig. 3, which demonstrates that the open structure does not adopt a conformation similar to the closed structure. The substantial difference between the average open *B. anthracis* structure during MD and the starting open crystal structure as well as the 3 ns required to equilibrate the open simulation, as seen in Fig. 3 *a*, suggest that the open structure may have crystallized in a conformation somewhat different from the one most favored in solution. The ability of the molecule to crystallize in this different, and apparently slightly energetically unfavorable, conformation is further evidence of the striking structural flexibility between the two domains. Furthermore, a slight energetic penalty associated with reaching the crystallized open conformation would be consistent with the difficulty encountered in crystallizing this form. A careful analysis of crystal contacts did not reveal any significant interaction that could be associated in a straightforward manner with favorable selection of the crystallized open structure of this enzyme. Therefore, it is also possible that the crystallization condition has some influence on this structure selection process.

As discussed above and depicted in Fig. 3 there appears to be no evidence of the enzyme opening up during the simulation starting at the closed structure. Equally, the simulation starting with the open structure did not approach the closed structure within the period of the simulation. No opening was seen even in the simulation in which 2PGA was removed from the closed structure before the run commencing. Comparable studies, based on MD trajectories of comparable length, often highlight domain motions in full agreement with multiple crystallized conformations (e.g., de Groot et al. (59) and Mello et al. (60)). This fact, combined with the ability of even subnanosecond simulations to effectively sample essential modes (61) and the overlap between MD and NMR ensemble-derived EDs eigenvectors (62), meant that the lack of movement of one structure toward the other was surprising and intriguing. Our results can be interpreted as follows. First, the lack of opening of the closed *B. stearothermophilus* structure during the simulation suggests that a significant kinetic barrier must exist for the opening to occur and that this barrier was not surmounted during the period of the MD. Second, since the Mn^{2+} ions are present in the open *B. anthracis* structure, its lack of closure could perhaps be explained by the absence of substrate. Such a profound effect of the presence of a bound substrate on protein dynamics would be expected as the substrate binds between the two domains, and both domains are necessary for catalysis. Transient binding of substrate to one domain would clearly assist domain closure since a favorable electrostatic interaction would exist between the substrate and the other domain.

The crystallographic and MD studies support the following scenario regarding the dynamic and structural properties of bacterial iPGMs: i), the substrate/product bound to the iPGM molecule triggers formation of the closed conformation, and ii), in the PGA-free form the enzyme assumes an open conformation. The data from x-ray, MD, and crystallization studies suggest that the iPGM mechanism follows the following scheme: i), in the PGA-free state the enzyme assumes an open conformation as illustrated by the current structure, ii), upon substrate binding the enzyme closes to the catalytically functional conformation as illustrated by the *B. stearothermophilus* iPGM-PGA structures, iii), in the closed form the enzyme catalyzes 2/3PGA isomerization resulting in product release, and iv), product release causes opening of the enzyme and return to the open conformation.

Further analyses were performed to better understand the PGA and Mn^{2+} movements in the MD simulations. Distances were measured between the PGA and Mn^{2+} ions and selected residues that contact with them in the crystal structures. No significant differences were found in these values for Mn^{2+} ions and their contact residues, and thus the Mn^{2+} coordination geometry remains unchanged throughout the simulation. However, during the course of the 10-ns simulation, the PGA dissociated from most residues to which it is bound in the crystal structure. For example, the distances from side-chain nitrogen atoms of Arg-261 and its neighboring residue Arg-191 (*B. stearothermophilus* numbering scheme in this entire paragraph) to phosphate oxygen atoms of PGA increased from 2.8–3.0 Å to 5.5 and 12 Å, respectively (Fig. 2 *c*). Arg-260 has been proposed to be involved in an essential bidentate interaction with the substrate/product phosphate group and to be responsible for the retention of the absolute configuration of this phosphate group during catalysis (6,7). Similar changes were observed for the protein's interactions with the substrate's carboxylate (bidentate interaction Arg-264-PG's carboxylate) and the remaining hydroxyl groups of PGA with Asp-154. They are similarly lost within 10 ns of simulation. The separation of Arg-264 side-chain nitrogen atoms and PGA carboxylate oxygen atoms increased from 2.7 and 3.0 Å (distances involving NE and NH2 atoms, respectively) in the initial structure to 5.5 and 6.0 Å by the end of the simulation. The corresponding Asp-154 to PGA hydroxyl distance initially measuring 2.7 Å (OD1 to 2PGA's OH) and it increased to the final value of 6.1 Å. The critical Arg-264-PGA carboxylate bidentate interaction was implicated in repositioning the glycerate moiety during catalysis (essential functional aspect of the transferase domain), whereas Asp-154 was involved in removal of the hydrogen from the PGA's OH group to allow nucleophilic attack on the phosphate group of the phospho-Ser intermediate, thus completing phosphate transfer (guided by and with retained orientation due to Arg-261-phosphate bidentate interaction) to the repositioned glycerate (6,7). The single exception was Ser-62, which remains at a similar distance due to its strong interaction with catalytic Mn^2. Mn^1, on the other hand, was directly implicated in the creation of the phospho-Ser intermediate and was a source of strong interactions with the phosphate group of the PGA substrate/product (6,7) that is retained in the catalytic site throughout the entire cycle of MD simulations. In both the *B. stearothermophilus* and *B. anthracis* iPGMs, both Mn^{2+} ions retain their coordination sphere geometry during the MD simulations. For *B. stearothermophilus* iPGM Mn^1 and Mn^2 always had square pyramidal coordination geometry and for *B. anthracis* iPGM Mn^1 had square pyramidal and Mn^2 octahedral arranged coordination sphere.

Although speculative, it can be suggested that the loss of interactions between PGA and key enzyme residues may be the first step in PGA dissociation from the enzyme. The relative instability of the PGA binding mode observed in the crystal is consistent with a relatively weak binding affinity for these molecules, as suggested by the rather high K_m values of the enzyme for substrates (4,8). At the same time, the lack of Mn^{2+} dissociation from the enzyme confirms that the binding of both Mn^{2+} ions was strong and essential for catalysis (4,8).

CONCLUSIONS

The *B. anthracis* iPGM crystal structure is significantly different from that of *B. stearothermophilus* iPGM, but the individual domains as well as catalytic residues and catalytic mechanisms are similar. The *B. anthracis* iPGM structure has a high degree of dynamic intramolecular interdomain motion and highlights the role of this enzyme's flexibility during its catalytic cycle. The new coordination geometry of the two Mn^{2+} ions in *B. anthracis* iPGM allows further insight into the pH-dependent regulation of iPGM function during spore formation and spore germination. Since iPGM catalysis requires precise active site positioning of substrate and involves direct interactions with both Mn^{2+} ions, changes in the Mn^{2+} ion's coordination geometry can directly affect catalysis and facilitate the regulation of iPGM activity by pH.

An understanding of the properties of *B. anthracis* iPGM enables the design of molecules of therapeutic utility against spores/germination spores or other bacteria utilizing this molecular form of iPGM.

The authors thank Dr. R. Keith Henderson for his help with the diffraction data collection. The diffraction data were collected at beamline 5.0.1 of the Berkeley Center for Structural Biology, Advanced Light Source, Lawrence Berkeley National Laboratory.

This work was supported by Defense Advanced Research Projects Agency contract N66001-01-C-8013 (to T.J.L., P.S., and M.J.J.). The coordinates and structure factors have been deposited in the Protein Data Bank with accession Nos. 2IFY and RCSB039528, respectively.

REFERENCES

1. Jedrzejas, M. J. 2000. Structure, function, and evolution of phosphoglycerate mutases: comparison with fructose-2,6-bisphosphatase, acid

phosphatase, and alkaline phosphatase. *Prog. Biophys. Mol. Biol.* 73: 263–287.

2. Fothergill-Gilmore, L. A., and H. C. Watson. 1989. The phosphoglycerate mutases. *Adv. Enzymol. Relat. Areas Mol. Biol.* 62:227–313.
3. Setlow, P., and A. Kornberg. 1970. Biochemical studies of bacterial sporulation and germination. XXII. Energy metabolism in early stages of germination of *Bacillus megaterium* spores. *J. Biol. Chem.* 245: 3637–3644.
4. Chander, M., B. Setlow, and P. Setlow. 1998. The enzymatic activity of phosphoglycerate mutase from gram-positive endospore-forming bacteria requires Mn^{2+} and is pH sensitive. *Can. J. Microbiol.* 44: 759–767.
5. Kuhn, N. J., B. Setlow, and P. Setlow. 1993. Manganese(II) activation of 3-phosphoglycerate mutase of *Bacillus megaterium*: pH-sensitive interconversion of active and inactive forms. *Arch. Biochem. Biophys.* 306:342–349.
6. Jedrzejas, M. J., M. Chander, P. Setlow, and G. Krishnasamy. 2000. Structure and mechanism of action of a novel phosphoglycerate mutase from *Bacillus stearothermophilus*. *EMBO J.* 19:1419–1431.
7. Jedrzejas, M. J., M. Chander, P. Setlow, and G. Krishnasamy. 2000. Mechanism of catalysis of the cofactor-independent phosphoglycerate mutase from *Bacillus stearothermophilus*. Crystal structure of the complex with 2-phosphoglycerate. *J. Biol. Chem.* 275:23146–23153.
8. Chander, M., P. Setlow, E. Lamani, and M. J. Jedrzejas. 1999. Structural studies on a 2,3-diphosphoglycerate independent phosphoglycerate mutase from *Bacillus stearothermophilus*. *J. Struct. Biol.* 126:156–165.
9. Kim, E. E., and H. W. Wyckoff. 1991. Reaction mechanism of alkaline phosphatase based on crystal structures. Two-metal ion catalysis. *J. Mol. Biol.* 218:449–464.
10. Bond, C. S., P. R. Clements, S. J. Ashby, C. A. Collyer, S. J. Harrop, J. J. Hopwood, and J. M. Guss. 1997. Structure of a human lysosomal sulfatase. *Structure*. 5:277–289.
11. Lukatela, G., N. Krauss, K. Theis, T. Selmer, V. Gieselmann, K. von Figura, and W. Saenger. 1998. Crystal structure of human arylsulfatase A: the aldehyde function and the metal ion at the active site suggest a novel mechanism for sulfate ester hydrolysis. *Biochemistry*. 37: 3654–3664.
12. Galperin, M. Y., and M. J. Jedrzejas. 2001. Conserved core structure and active site residues in alkaline phosphatase superfamily enzymes. *Proteins Struct Funct Genet.* 45:318–324.
13. Breathnach, R., and J. R. Knowles. 1977. Phosphoglycerate mutase from wheat germ: studies with ^{18}O-labeled substrate, investigations of the phosphatase and phosphoryl transfer activities, and evidence for a phosphoryl-enzyme intermediate. *Biochemistry.* 16:3054–3060.
14. Leadlay, P. F., R. Breathnach, J. A. Gatehouse, P. E. Johnson, and J. R. Knowles. 1977. Phosphoglycerate mutase from wheat germ: studies with isotopically labeled 3-phospho-D-glycerates showing that the catalyzed reaction is intramolecular. Appendix: phosphoglycerate mutase from wheat germ: isolation, crystallization, and properties. *Biochemistry.* 16:3045–3053.
15. Britton, H. G., J. Carreras, and S. Grisolia. 1971. Mechanism of action of 2,3-diphosphoglycerate-independent phosphoglycerate mutase. *Biochemistry.* 10:4522–4533.
16. Harding, M. M. 1999. The geometry of metal-ligand interactions relevant to proteins. *Acta Crystallogr. D Biol. Crystallogr.* 55:1432–1443.
17. Jedrzejas, M. J., and P. Setlow. 2001. Comparison of the binuclear metalloenzymes diphosphoglycerate-independent phosphoglycerate mutase and alkaline phosphatase: their mechanism of catalysis via a phosphoserine intermediate. *Chem. Rev.* 101:607–618.
18. Jedrzejas, M. J. 2002. The structure and function of novel proteins of *Bacillus anthracis* and other spore-forming bacteria: development of novel prophylactic and therapeutic agents. *Crit. Rev. Biochem. Mol. Biol.* 37:339–373.
19. Jedrzejas, M. 2002. Three-dimensional structure and molecular mechanism of novel enzymes of spore-forming bacteria. *Med. Sci. Monit.* 8:183–190.
20. Leyva-Vazquez, M. A., and P. Setlow. 1994. Cloning and nucleotide sequences of the genes encoding triose phosphate isomerase, phosphoglycerate mutase, and enolase from *Bacillus subtilis*. *J. Bacteriol.* 176:3903–3910.
21. Oh, Y. K., and E. Freese. 1976. Manganese requirement of phosphoglycerate phosphomutase and its consequences for growth and sporulation of *Bacilus subtilis*. *J. Bacteriol.* 127:739–746.
22. Pearson, C. L., C. A. Loshon, L. B. Pedersen, B. Setlow, and P. Setlow. 2000. Analysis of the function of a putative 2,3-diphosphoglyceric acid-dependent phosphoglycerate mutase from *Bacillus subtilis*. *J. Bacteriol.* 182:4121–4123.
23. Rigden, D. J., I. Bagyan, E. Lamani, P. Setlow, and M. J. Jedrzejas. 2001. A cofactor-dependent phosphoglycerate mutase homolog from *Bacillus stearothermophilus* is actually a broad specificity phosphatase. *Protein Sci.* 10:1835–1846.
24. Rigden, D. J., E. Lamani, L. V. Mello, J. E. Littlejohn, and M. J. Jedrzejas. 2003. Insights into the catalytic mechanism of cofactor-independent phosphoglycerate mutase from x-ray crystallography, simulated dynamics and molecular modeling. *J. Mol. Biol.* 328:909–920.
25. Rigden, D. J., J. E. Littlejohn, K. Henderson, and M. J. Jedrzejas. 2003. Structures of phosphate and trivanadate complexes of *Bacillus stearothermophilus* phosphatase PhoE: structural and functional analysis in the cofactor-dependent phosphoglycerate mutase superfamily. *J. Mol. Biol.* 325:411–420.
26. Rigden, D. J., L. V. Mello, P. Setlow, and M. J. Jedrzejas. 2002. Structure and mechanism of action of a cofactor-dependent phosphoglycerate mutase homolog from *Bacillus stearothermophilus* with broad specificity phosphatase activity. *J. Mol. Biol.* 315:1129–1143.
27. Read, T. D., S. N. Peterson, N. Tourasse, L. W. Baillie, I. T. Paulsen, K. E. Nelson, H. Tettelin, D. E. Fouts, J. A. Eisen, S. R. Gill, E. K. Holtzapple, O. A. Okstad, E. Helgason, J. Rilstone, M. Wu, J. F. Kolonay, M. J. Beanan, R. J. Dodson, L. M. Brinkac, M. Gwinn, R. T. DeBoy, R. Madpu, S. C. Daugherty, A. S. Durkin, D. H. Haft, W. C. Nelson, J. D. Peterson, M. Pop, H. M. Khouri, D. Radune, J. L. Benton, Y. Mahamoud, L. Jiang, I. R. Hance, J. F. Weidman, K. J. Berry, R. D. Plaut, A. M. Wolf, K. L. Watkins, W. C. Nierman, A. Hazen, R. Cline, C. Redmond, J. E. Thwaite, O. White, S. L. Salzberg, B. Thomason, A. M. Friedlander, T. M. Koehler, P. C. Hanna, A. B. Kolsto, and C. M. Fraser. 2003. The genome sequence of *Bacillus anthracis* Ames and comparison to closely related bacteria. *Nature*. 423:81–86.
28. Schlapfer, B. S., and H. Zuber. 1992. Cloning and sequencing of the genes encoding glyceraldehyde-3-phosphate dehydrogenase, phosphoglycerate kinase and triosephosphate isomerase (gap operon) from mesophilic *Bacillus megaterium*: comparison with corresponding sequences from thermophilic *Bacillus stearothermophilus*. *Gene*. 122: 53–62.
29. LaVallie, E. R., E. A. DiBlasio, S. Kovacic, K. L. Grant, P. F. Schendel, and J. M. McCoy. 1993. A thioredoxin gene fusion expression system that circumvents inclusion body formation in the *E. coli* cytoplasm. *Biotechnology (N. Y.).* 11:187–193.
30. Sambrook, J., E. T. Fritsch, and T. Maniatis. 1989. Molecular Cloning: A Laboratory Manual. Cold Spring Harbor Laboratory Press, Cold Spring Harbor, NY.
31. Chong, S., F. B. Mersha, D. G. Comb, M. E. Scott, D. Landry, L. M. Vence, F. B. Perler, J. Benner, R. B. Kucera, C. A. Hirvonen, J. J. Pelletier, H. Paulus, and M. Q. Xu. 1997. Single-column purification of free recombinant proteins using a self-cleavable affinity tag derived from a protein splicing element. *Gene*. 192:271–281.
32. Laemmli, U. K. 1970. Cleavage of structural proteins during the assembly of the head of bacteriophage T4. *Nature*. 227:680–685.
33. McPherson, A. 1999. Crystallization of Biological Macromolecules. Cold Spring Harbor Laboratory Press, Cold Spring Harbor, New York.
34. Otwinowski, Z., and W. Minor. 1997. Processing of x-ray diffraction data collected in oscillation mode. *Methods Enzymol.* 276:307–326.
35. McCoy, A. J., R. W. Grosse-Kunstleve, L. C. Storoni, and R. J. Read. 2005. Likelihood-enhanced fast translation functions. *Acta Crystallogr. D Biol. Crystallogr.* 61:458–464.

36. Storoni, L. C., A. J. McCoy, and R. J. Read. 2004. Likelihood-enhanced fast rotation functions. *Acta Crystallogr. D Biol. Crystallogr.* 60:432–438.

37. Collaborative Computational Project, Number 4. 1994. The CCP4 suite: programs for protein crystallography. *Acta Crystallogr. D Biol. Crystallogr.* 50:760–763.

38. Jones, T. A., J. Y. Zou, S. W. Cowan, and M. Kjeldgaard. 1991. Improved methods for binding protein models in electron density maps and the location of errors in these models. *Acta Crystallogr. A.* 47: 110–119.

39. Read, R. J. 1986. Improved Fourier coefficients for maps using phases from partial structures with errors. *Acta Crystallogr. A.* 42:140–149.

40. Brunger, A. T. 1992. Free R value: a novel statistical quantity for assessing the accuracy of crystal structures. *Nature.* 355:472–475.

41. Laskowski, R. A., M. W. MacArthur, D. S. Moss, and J. M. Thornton. 1993. PROCHECK: a program to check the stereochemical quality of protein structures. *J. Appl. Crystallogr.* 26:283–291.

42. Vaguine, A. A., J. Richelle, and S. J. Wodak. 1999. SFCHECK: a unified set of procedures for evaluating the quality of macromolecular structure-factor data and their agreement with the atomic model. *Acta Crystallogr. D Biol. Crystallogr.* 55:191–205.

43. DeLano, W. L. 2005. The PyMOL Molecular Graphics System. DeLano Scientific, San Carlos, CA. pymol.sourceforge.net.

44. Nicholls, A., K. A. Sharp, and B. Honig. 1991. Protein folding and association: insights from the interfacial and thermodynamic properties of hydrocarbons. *Proteins Struct Funct Genet.* 11:281–296.

45. Lindahl, E., B. Hess, and D. van der Spoel. 2001. GROMACS 3.0: a package for molecular simulation and trajectory analysis. *J. Mol. Model. (Online).* 7:306–317.

46. Schuttelkopf, A. W., and D. M. van Aalten. 2004. PRODRG: a tool for high-throughput crystallography of protein-ligand complexes. *Acta Crystallogr. D Biol. Crystallogr.* 60:1355–1363.

47. Hayward, S., and R. A. Lee. 2002. Improvements in the analysis of domain motions in proteins from conformational change: DynDom version 1.50. *J. Mol. Graph. Model.* 21:181–183.

48. Hayward, S., and H. J. Berendsen. 1998. Systematic analysis of domain motions in proteins from conformational change: new results on citrate synthase and T4 lysozyme. *Proteins Struct Funct Genet.* 30:144–154.

49. Bucher, T., W. Lu, and D. Pette. 1964. Assay of phosphoglycerate mutase. *In* Hoppe-Seyler/Thiefelder, Handbuch der physiologisch und pathogisch-chemischen analyse. K. Long, editor. Springer-Verlag, Berlin. 292–339.

50. Pace, C. N., F. Vajdos, L. Fee, G. Grimsley, and T. Gray. 1995. How to measure and predict the molar absorption coefficient of a protein. *Protein Sci.* 4:2411–2423.

51. Lamani, E., D. T. McPherson, S. K. Hollingshead, and M. J. Jedrzejas. 2000. Production, characterization, and crystallization of truncated forms of pneumococcal surface protein A from *Escherichia coli*. *Protein Expr. Purif.* 20:379–388.

52. Sternberg, M. J., F. E. Cohen, W. R. Taylor, and R. J. Feldmann. 1981. Analysis and predication of structural motifs in the glycolytic enzymes. *Philos. Trans. R. Soc. Lond. B Biol. Sci.* 293:177–189.

53. Cotton, F. A. 1980. Advanced Inorganic Chemistry. G. Wilkinson, editor. Wiley, New York.

54. Swerdlow, B. M., B. Setlow, and P. Setlow. 1981. Levels of H+ and other monovalent cations in dormant and germinating spores of *Bacillus megaterium*. *J. Bacteriol.* 148:20–29.

55. Magill, N. G., A. E. Cowan, M. A. Leyva-Vazquez, M. Brown, D. E. Koppel, and P. Setlow. 1996. Analysis of the relationship between the decrease in pH and accumulation of 3-phosphoglyceric acid in developing forespores of *Bacillus* species. *J. Bacteriol.* 178:2204–2210.

56. Magill, N. G., A. E. Cowan, D. E. Koppel, and P. Setlow. 1994. The internal pH of the forespore compartment of *Bacillus megaterium* decreases by about 1 pH unit during sporulation. *J. Bacteriol.* 176:2252–2258.

57. Sun, L., E. R. Kantrowitz, and W. C. Galley. 1997. Room temperature phosphorescence study of phosphate binding in *Escherichia coli* alkaline phosphatase. *Eur. J. Biochem.* 245:32–39.

58. Bucevic-Popovic, V., M. Pavela-Vrancic, and R. Dieckmann. 2004. Metal-ion induced conformational changes in alkaline phosphatase from *E. coli* assessed by limited proteolysis. *Biochimie.* 86:403–409.

59. de Groot, B. L., S. Hayward, D. M. van Aalten, A. Amadei, and H. J. Berendsen. 1998. Domain motions in bacteriophage T4 lysozyme: a comparison between molecular dynamics and crystallographic data. *Proteins Struct Funct Genet.* 31:116–127.

60. Mello, L. V., B. L. de Groot, S. Li, and M. J. Jedrzejas. 2002. Structure and flexibility of *Streptococcus agalactiae* hyaluronate lyase complex with its substrate. Insights into the mechanism of processive degradation of hyaluronan. *J. Biol. Chem.* 277:36678–36688.

61. Amadei, A., M. A. Ceruso, and A. Di Nola. 1999. On the convergence of the conformational coordinates basis set obtained by the essential dynamics analysis of proteins' molecular dynamics simulations. *Proteins Struct Funct Genet.* 36:419–424.

62. Abseher, R., L. Horstink, C. W. Hilbers, and M. Nilges. 1998. Essential spaces defined by NMR structure ensembles and molecular dynamics simulation show significant overlap. *Proteins Struct Funct Genet.* 31:370–382.